Semiconductors

International Edition: DOI: 10.1002/anie.201504764
German Edition: DOI: 10.1002/ange.201504764

Electroless Deposition of III–V Semiconductor Nanostructures from Ionic Liquids at Room Temperature

Abhishek Lahiri, Natalia Borisenko,* Mark Olschewski, René Gustus, Janine Zahlbach, and Frank Endres*

Abstract: *Group III–V semiconductor nanostructures are important materials in optoelectronic devices and are being researched in energy-related fields. A simple approach for the synthesis of these semiconductors with well-defined nanostructures is desired. Electroless deposition (galvanic displacement) is a fast and versatile technique for deposition of one material on another and depends on the redox potentials of the two materials. Herein we show that GaSb can be directly synthesized at room temperature by galvanic displacement of $SbCl_3$/ionic liquid on electrodeposited Ga, on Ga nanowires, and also on commercial Ga. In situ AFM revealed the galvanic displacement process of Sb on Ga and showed that the displacement process continues even after the formation of GaSb. The bandgap of the deposited GaSb was 0.9 ± 0.1 eV compared to its usual bandgap of 0.7 eV. By changing the cation in the ionic liquid, the redox process could be varied leading to GaSb with different optical properties.*

GaSb is an interesting III–V semiconductor and has been considered in devices, such as laser diodes,[1] transistors,[2] photodetectors,[3] solar cells. [4] Extensive studies on growing GaSb crystals using the Czochralski technique and Bridgeman technique have been made.[5] For thin-film/epitaxial growth, techniques, such as chemical vapor deposition (CVD), molecular beam epitaxy (MBE), vapor phase epitaxy (VPE) are used.[6] All these techniques use high-temperature ($>500\,°C$) and high-vacuum conditions ($<10^{-6}$ Torr). It has been shown that working at high temperatures and vacuum conditions leads to formation of Ga_2O_3, dissociation of GaSb, and loss of Sb atoms at about 2×10^{15} atoms per second.[6,7] With these limitations, a near room-temperature synthesis route would be advantageous.

An electrochemical route, especially electrodeposition, is an attractive and viable technique to deposit semiconductors. In electrodeposition, an external power source is used to deposit the material and the composition of the deposit is controlled by the applied potential/current. For formation of an alloy, the reduction rates play a pivotal role for alloying as well as in defining the composition. GaSb can be electrodeposited at temperatures of 80 °C from aqueous solutions.[8] However, problems related to hydrogen evolution during the electrodeposition of Ga and Sb occur.[8] In comparison, ionic liquids are a class of electrolytes which have been found to be good solvents for the electrodeposition of metals and semiconductors.[9] There are very few reports on the electrodeposition of antimonide compounds, for example, AlSb, InSb, and AlInSb from ionic liquids at room temperature.[10] An alternative approach to electrodeposition would be to trigger a redox reaction (galvanic displacement) between two metals and facilitate the formation of alloys. In galvanic displacement reactions from aqueous solutions, a more-noble metal can be deposited on a less-noble metal. Abbott et al.[11a,b] were the first to show galvanic displacement in ionic liquids wherein metallic silver was deposited on copper. However, in ionic liquids, it was shown that Ga can displace a more-noble metal, such as Au, at room temperature and form a Ga thin film on Au.[11c] Usually, controlling the galvanic displacement reaction is limited to changes in the concentrations of ions and temperature. An interesting aspect of ionic liquids is that their electrochemical behavior depends on the cation and anion species.[12] Therefore choice of cation and anion becomes important as it can be used to govern the reduction rates, thereby assisting in controlling the composition of the alloys.

Taking these factors into consideration, we show herein for the first time that galvanic displacement can be used to prepare GaSb semiconductors at room temperature. For the formation of GaSb, a difference in redox potentials between Sb and Ga in the ionic liquid is required. As the solid-state diffusion coefficient of Ga in amorphous Sb is $2\times10^{-20}\,m^2s^{-1}$ at 20 °C,[8] it would take a few hundred seconds for Ga to diffuse in Sb on the nanometer scale. If the deposition rate of Sb can be controlled in such a way that gallium diffuses in Sb quickly, it would lead to the direct formation of GaSb.

To verify the feasibility of the electroless deposition of GaSb, the open circuit potential (OCP) of electrodeposited Sb and Ga was evaluated in the ionic liquids 1-butyl-1-methylpyrrolidinium bis(trifluoromethylsulfonyl)amide ($[Py_{1,4}]$TFSA) and 1-ethyl-3-methylimidazolium bis(trifluoromethylsulfonyl)amide ([Emim]TFSA). Figure 1a shows the OCP change over 120 seconds. The OCP of Ga in $[Py_{1,4}]$TFSA and [Emim]TFSA is −1.02 V and −0.86 V vs. Pt, respectively, whereas that of Sb is −0.78 V and −0.62 V vs. Pt in $[Py_{1,4}]$TFSA and [Emim]TFSA, respectively. To exclude any influence by a "real" reference electrode such as Ag/Ag-(CF_3SO_3), we decided to use a Pt quasi-reference electrode which showed sufficient stability. It is evident that there is some change in OCP with time in the ionic liquids which

[*] Dr. A. Lahiri, Dr. N. Borisenko, M. Olschewski, R. Gustus, J. Zahlbach, Prof. Dr. F. Endres
Institute of Electrochemistry
Clausthal University of Technology
Arnold-Sommerfeld-Strasse 6, 38678 Clausthal-Zellerfeld (Germany)
E-mail: abhishek.lahiri@tu-clausthal.de
natalia.borissenko@tu-clausthal.de

Supporting information for this article is available on the WWW under http://dx.doi.org/10.1002/anie.201504764.

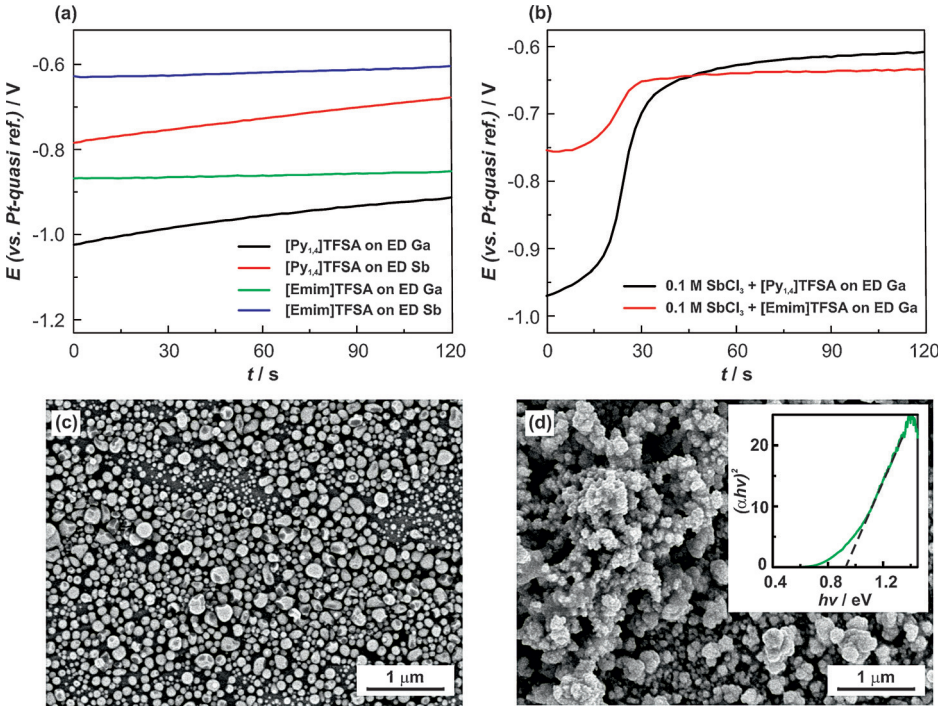

Figure 1. a) OCP of electrodeposited (ED) Ga and Sb in $[Py_{1,4}]$TFSA and [Emim]TFSA. b) Change in OCP on addition of 0.1 M $SbCl_3$-$[Py_{1,4}]$TFSA and 0.1 M $SbCl_3$-[Emim]TFSA on electrodeposited Ga. c) SEM of electrodeposited Ga from 0.1 M $GaCl_3$-$[Py_{1,4}]$TFSA. d) SEM of electroless deposited Sb for 2 min on electrodeposited Ga from 0.1 M $SbCl_3$-$[Py_{1,4}]$TFSA. Inset: the direct bandgap of GaSb calculated using Tauc plot.

could be related to corrosion/passivation of Ga and Sb. However, as the OCP on Ga is more negative compared to that on Sb, galvanic displacement of Sb onto Ga will take place. Figure 1 b shows the change in OCP on addition of 0.1M $SbCl_3$-$[Py_{1,4}]$TFSA and of 0.1M $SbCl_3$-[Emim]TFSA on the electrodeposited Ga from their respective ionic liquids. On addition of 0.1M $SbCl_3$-$[Py_{1,4}]$TFSA, it is evident that after some incubation period of about 15 s, there is a rapid change in the potential from −0.9 V to −0.65 V after which the curve plateaus. On addition of 0.1M $SbCl_3$-[Emim]TFSA, the change in potential is from −0.75 V to −0.66 V which is considerably less than that of $[Py_{1,4}]$TFSA. This difference indicates that the change in the cation of the ionic liquid has an effect on the deposition process.

Repeated experiments showed that the incubation period and OCP change vary during the galvanic displacement reaction (Figure S1,S2 in the Supporting Information) which can arise from the difference in the kinetics of the reaction. However, there might be some error in the potential change caused by the use of Pt quasi reference electrode. However, during in situ AFM studies (see below) we don't use a Pt reference electrode, so we are sure that the change in the OCP can only be related to the galvanic displacement reaction. Furthermore, to relegate the possibility of the Cu substrate triggering the reaction or acting as a catalyst, experiments were also performed on glassy carbon and a similar OCP change was observed (Figure S1) confirming that there is an electroless deposition of Sb taking place on electrodeposited Ga. During the deposition, a color change of the electrodeposit was noted from gray to black. To confirm that a galvanic displacement reaction took place, induction coupled plasma-optical emission spectroscopy (ICP-OES) was performed on the electrolyte and the concentration of Ga was found to be 7.5 $mg\,L^{-1}$.

The SEM of the electrodeposited Ga from 0.1M $GaCl_3$-$[Py_{1,4}]$TFSA shows spherical morphology with variable particle sizes between 30 and 70 nm (Figure 1 c). After electroless deposition of Sb, a change in morphology to a clustered growth is evident (Figure 1 d). A similar observation was made on electrodepositing Ga from [Emim]TFSA (Figure S3a), for which a spherical morphology was observed, and on depositing Sb by galvanic displacement process, irregular particles were seen (Figure S3b). X-ray diffraction of the deposit did not reveal any crystalline structures. From UV/Vis reflectance spectroscopic measurements, the bandgap of the deposit was determined. As a thin layer of residual ionic liquid usually covers the deposit even after washing in isopropanol, the deposit was sputtered by Ar^+ ions (1 keV) in an ultra-high vacuum (UHV) chamber before analysis. From the reflectance spectra (Figure S4), a clear absorption is seen in the near-infrared region from 0.6 eV for the samples deposited from both $[Py_{1,4}]$TFSA and [Emim]TFSA. The absorption intensity is higher in the case of [Emim]TFSA and plateaus around 1.2 eV whereas for GaSb deposited from $[Py_{1,4}]$TFSA, the absorption plateaus around 0.9 eV. This situation indicates that the deposition was influenced by a change in the reaction kinetics caused by the cation. The direct bandgap calculated using Tauc plot for GaSb deposited from $[Py_{1,4}]$TFSA is shown in the inset in Figure 1 d and was found to be 0.93 eV. GaSb has a bandgap between 0.68 and 0.72 eV. However, in very small particles it shows quantum confinement effects.[13] In quantum-confined GaSb, an increase in bandgap is expected which is consistent with the higher bandgap obtained in electroless deposition. However, different Ga_xSb_{1-x} species could also form in the electroless process and alter the bandgap.

To identify the formation of GaSb and to understand the chemical composition along the depth of the deposit, X-ray photoelectron spectroscopy (XPS) and Auger electron spectroscopy (AES) were used. The survey spectra of the as-deposited GaSb and after sputtering for various times are shown in Supporting Information (Figure S5). Both Ga and Sb could be detected in the survey spectra after sputtering . Carbon, chlorine and small amounts of fluorine were also

found indicating the presence of some residual electrolyte or its decomposed products. The Cu and Mo peaks are from the substrate and XPS sample holder, respectively.

The XPS detail spectra of Ga $2p^{3/2}$ and Sb $3d^{5/2}$ (black dots) including Gauss-Lorentzian line fits (green and blue lines) are shown in Figure 2a,b. To fit the Sb 3d spectrum both

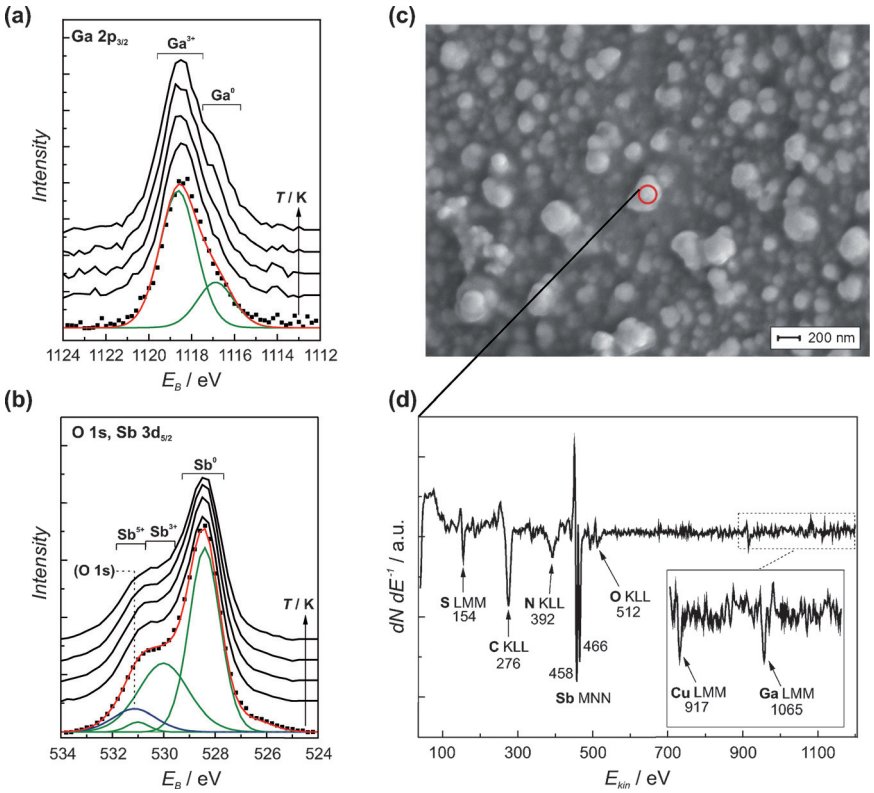

Figure 2. a,b) XPS detail spectrum (black dots) with component peak fits (green and blue) and changes during annealing from RT to 395 K of Ga $2p^{3/2}$ (a) and Sb $3d^{5/2}$ region (b); red line to guide the eye. c) SEM image of GaSb recorded at a beam energy of 5 kV, 1.5 nA. d) AES spectrum of the particle marked in the SEM image.

5/2 and 3/2 spin-orbit components were taken into account, as the O 1s signal overlaps with Sb $3d^{5/2}$ region. While heating the sample from room temperature to 395 K, photoelectron spectra were continuously taken as shown in Figure 2a,b and are represented as a waterfall plot of black solid lines. The main peak of the Sb $3d^{5/2}$ spectrum at 528.4 eV can be assigned to metallic antimony (Sb^0) the peaks at 530 eV and 531 eV belong to Sb^{3+} and Sb^{5+} and indicate the presence of oxide species.[14] The small shoulder at approximately 526.5 eV might be related to slight peak anisotropy of Sb 3d. The Ga $2p^{3/2}$ spectrum in Figure 2b is fitted by two components at 1116.9 eV for metallic Ga^0 and 1118.6 eV for Ga^{3+} indicating oxide species. The presence of metallic Sb and metallic Ga in the spectrum clearly indicates the formation of GaSb and is consistent with the literature.[15]

To further clarify the formation of GaSb, heating experiments within the XPS chamber were performed. During heating, the growth of the shoulder of the metallic Ga^0 component in the Ga 2p peak is evident (Figure 2a). Meanwhile the intensity of the Sb 3d peak decreases (Figure 2b) indicating that there is a temperature-driven diffusion of gallium to the surface and possible desorption of Sb and Sb_2O_3 during annealing.

Raman spectra were performed on the deposited GaSb after annealing at 395 K in the XPS experiments. Electrodeposited Sb on the Cu substrate showed a Raman band at 175 cm^{-1} whereas for GaSb, in addition to Sb Raman bands, two distinct peaks at 228 cm^{-1} and 336 cm^{-1} were observed (Figure S6) which are characteristic of transverse (TO) and longitudinal (LO) optical lines for GaSb.[16] Although the composition analysis from XPS (Table S1) did not show 1:1 ratio for Ga to Sb owing to partial oxidation of the deposit, Raman Spectra and the bandgap clearly indicate the formation of GaSb. Thermodynamically, it has been shown that GaSb can coexist with Ga_2O_3 and elemental Sb[16] and therefore estimating the composition becomes difficult.

Figure 2c shows the SEM image of the sample after Ar^+ ion sputtering at room temperature. The surface consists of particles with variable diameters between 30 and 200 nm. No specific faceting is observed in the particles indicating amorphous GaSb. To obtain local information about the chemical composition of these particles, high resolution AES measurements were performed. The AES spectrum of one of the particles, marked in the SEM image in Figure 2c is shown in Figure 2d. In the spectrum distinctive peaks are shown at kinetic energies of 154, 276, 392, and 458/466 eV, which can be assigned to the S LMM, C KLL, N KLL and Sb MNN emission. In addition small peaks located at 512, 917, and 1065 eV can be identified, deriving from the O KLL, Cu LMM, and Ga LMM emission. According to the shape and kinetic energy of the Sb MNN peaks, antimony exists in the metallic state without any chemical bonding to oxygen or sulfur.[17] Thus, from the combination of spectroscopic analyses, we can confirm the formation of GaSb.

To observe the galvanic displacement reaction in real-time and determine the growth rate, in situ AFM was used. The snapshots in Figure 3 show the height and deflection images at various times. Some spherical gallium nanoparticles in the size range between 40 and 70 nm can be discerned (marked by arrows, Figure 3a) from the height and deflection images. After 3 min of the displacement process in a solution of 25 mM $SbCl_3$-$[Py_{1,4}]TFSA$ (Figure 3b), the growth in the nanoparticles is evident. From the topography and deflection images, the coagulated spherical shapes of the nanoparticles (marked by arrows) can clearly be seen. On continuing the deposition for 24 min (Figure 3c), the topography shows the formation

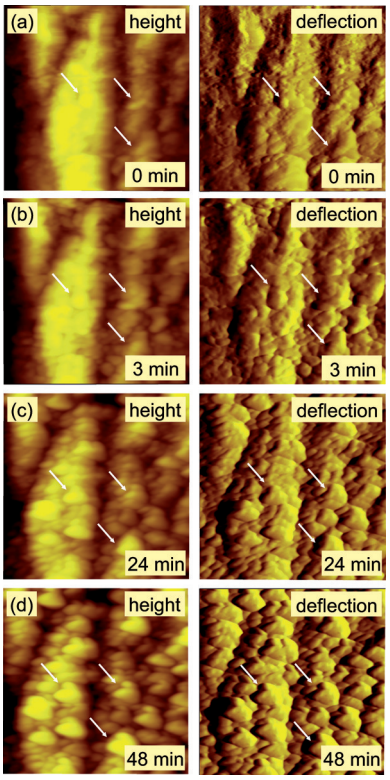

Figure 3. In situ AFM snapshots taken at various time intervals during galvanic displacement of Sb on electrodeposited Ga in 25 mM $SbCl_3$-$[Py_{1,4}]TFSA$, (2 μm × 2 μm) image.

of triangular plate-like structures, some having a size of about 250 nm.

Compared to initial gallium in Figure 3a, it is evident that the gallium is covered with Sb at this stage. However, interestingly the deposition process continues. Abbott et al.[11a,b] observed a similar phenomenon in case of electroless deposition of Ag on Cu and related the continuation of the deposition to the porous nature of the deposited Ag. However, no porosity is observed from both topography and deflection images in Figure 3. As Ga diffusion in Sb is fast,[8b] the continuation of the deposition process could be due to the diffusion of Ga from the bulk through the deposited Sb/GaSb layers. The diffused Ga then becomes oxidized on coming in contact with $SbCl_3$ in the ionic liquid and therefore the deposition process continues. XPS measurements in Figure S5 confirmed that Ga is present throughout the depth of the sample which confirms the fast diffusion of Ga in Sb. After 48 min of deposition, triangular/heart shaped structures were observed having a size of about 300 nm. All images were combined to a movie that is shown in the Supporting Information (S1 movie). The dimensional growth of a single particle marked by the arrows in Figure 3c was used to determine the deposition rate between 24 and 48 min. The deposition rate was estimated to be 0.3 nm min^{-1} along the height and 2.3 nm min^{-1} along the width (Figure S7). Repeated experiments showed that although electroless deposition takes place every time and a layer-by-layer growth is observed, the nucleation and growth process differs from experiment to experiment (S2 movie). This variation might have led to the difference in the change in OCP observed in Figure S1 and Figure S2. Thus, based on the AFM and XPS depth profile results, the formation of GaSb likely occurs by oxidation of Ga in the presence of Sb^{3+}-containing ionic liquid and simultaneous deposition of Sb.

As the galvanic displacement technique for the formation of GaSb thin films was effective, the same technique was also used to form GaSb nanowires. Figure 4a shows the topography and deflection images of Ga nanowires synthesized using template-assisted electrodeposition. The diameter of the nanowires is 90 nm and is consistent with the pore diameter of the polymer template. After 6 min of electroless deposition, it is evident from the topography and deflection images (Figure 4b) that the size of the nanowire has increased. From the topography, the height and the diameter of the nanowire was found to increase from 5 nm to about 9 nm and from 90 nm to about 140 nm, respectively as seen in Figure 4c.

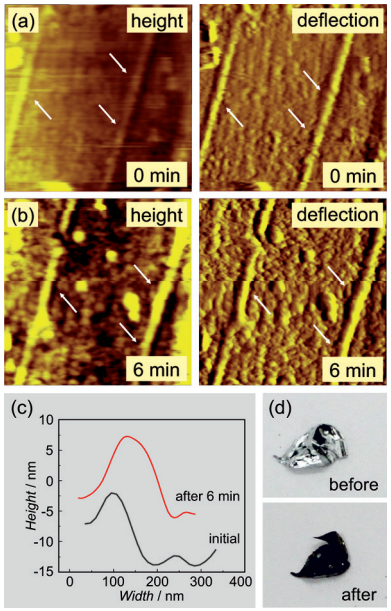

Figure 4. a) AFM image of Ga nanowires in $[Py_{1,4}]TFSA$. b) After 6 min of galvanic displacement of Sb on Ga nanowires in 25 mM $SbCl_3$-$[Py_{1,4}]TFSA$, (1.8 μm × 1.8 μm) image. c) Dimensions of the nanowire obtained from the height image. d) Commercial gallium before and after immersing in 0.1 M $SbCl_3$-$[Py_{1,4}]TFSA$.

To assess the possibility of commercial application, experiments were also performed on gallium obtained from Sigma–Aldrich. The gallium appeared shiny gray in color (Figure 4d) and once dipped in the ionic liquid with $SbCl_3$, it gave a blackish texture (Figure 4d). This shows that the process for synthesizing GaSb from ionic liquid is not limited to only electrodeposited Ga but also is viable on any gallium substrate.

In conclusion, we have shown a simple electroless technique for synthesizing GaSb nanostructures at room temperature. The formation of GaSb was confirmed by XPS, AES, and Raman spectroscopy techniques. The deposited

GaSb showed a bandgap of 0.93 ± 0.1 eV indicating a quantum-confinement effect. Also, it was shown that the choice of cation of the ionic liquid affects the deposition process and optical properties. Similar approach can be used to develop binary and ternary nanostructured semiconductor alloys using the galvanic displacement technique as long as there is a difference in OCP or reduction potentials between the materials. Furthermore, the reaction can be controlled by changing the cation and anion of the ionic liquids as well as the reaction temperature and concentration, giving ample amount of parameters for developing and controlling the alloys and its composition. Thus, the simple strategy used in this study opens up a new way to synthesize semiconductor nanostructures which could find applications in optoelectronic devices as well as energy related applications, such as solar cells and battery electrodes.

Acknowledgements

We thank Prof. W. Daum for providing the NanoSAM (Omicron NanoSAM provided by: Deutsche Forschungsgesellschaft DFG, grant number: INST 189/158-1) and also financial support from DFG, SPP 1708, grant number: BO 4290/1-1. We also thank Karin Bode for Raman measurements and Petra Lassen for ICP-OES measurements.

Keywords: electroless deposition · GaSb · AFM · ionic liquids · semiconductors

How to cite: *Angew. Chem. Int. Ed.* **2015**, *54*, 11870–11874
Angew. Chem. **2015**, *127*, 12038–12042

[1] A. Joullié, P. Christol, *C. R. Phys.* **2003**, *4*, 621–637.
[2] B. R. Bennett, R. Magno, J. B. Boos, W. Kruppa, M. G. Ancona, *Solid-State Electron.* **2005**, *49*, 1875–1895.
[3] Z. M. Zhu, P. Bhattacharya, E. Plis, X. H. Su, S. Krishna, *J. Phys. D* **2006**, *39*, 4997–5001.
[4] R. B. Laghumavarapu, A. Moscho, A. Khoshakhlagh, M. El-Emawy, L. F. Lester, D. L. Huffaker, *Appl. Phys. Lett.* **2007**, *90*, 173125.
[5] a) C. E. M. de Oliveira, M. M. G. de Carvalho, *J. Cryst. Growth* **1995**, *151*, 9–12; b) P. S. Dutta, K. S. Sangunni, H. L. Bhat, V. Kumar, *J. Cryst. Growth* **1994**, *141*, 44–50.
[6] a) P. S. Dutta, H. L. Bhat, V. Kumar, *J. Appl. Phys.* **1997**, *81*, 5821–5870; b) R. M. Biefeld, *Mater. Sci. Eng. R* **2002**, *36*, 105–142; c) B. M. Borg, L.-E. Wernersson, *Nanotechnology* **2013**, *24*, 202001.
[7] a) K. B. McAfee, D. M. Gay, R. S. Hozack, R. A. Laudise, G. Schwartz, W. A. Sunder, *J. Cryst. Growth* **1986**, *76*, 263–271; b) W. A. Sunder, R. L. Barns, T. Y. Kometani, J. M. Parsey, Jr., R. A. Laudise, *J. Cryst. Growth* **1986**, *78*, 9–18.
[8] a) J.-J. McChesney, J. Haigh, I. M. Dharmadasa, D. J. Mowthorpe, *Opt. Mater.* **1996**, *6*, 63–67; b) V. M. Kozlov, L. P. Bicelli, *J. Alloys Compd.* **2000**, *313*, 161–167.
[9] a) F. Endres, *ChemPhysChem* **2002**, *3*, 144–154; b) M. Armand, F. Endres, D. R. MacFarlane, H. Ohno, B. Scrosati, *Nat. Mater.* **2009**, *8*, 621–629.
[10] a) O. Mann, W. Freyland, *Electrochim. Acta* **2007**, *53*, 518–524; b) T. Tsuda, C. L. Hussey, *Thin Solid Films* **2008**, *516*, 6220–6225.
[11] a) A. P. Abbott, S. Nandhra, S. Postlethwaite, E. L. Smith, K. S. Ryder, *Phys. Chem. Chem. Phys.* **2007**, *9*, 3735–3743; b) A. P. Abbott, J. Griffith, S. Nandhra, C. O'Connor, S. Postlethwaite, K. S. Ryder, E. L. Smith, *Surf. Coat. Technol.* **2008**, *202*, 2033–2039; c) L. H. S. Gasparotto, N. Borisenko, O. Höfft, R. Al-Salman, W. Maus-Friedrichs, N. Bocchi, S. Zein El Abedin, F. Endres, *Electrochim. Acta* **2009**, *55*, 218–226.
[12] F. Endres, O. Höfft, N. Borisenko, L. H. Gasparotto, A. Prowald, R. Al-Salman, T. Carstens, R. Atkin, A. Bund, S. Zein El Abedin, *Phys. Chem. Chem. Phys.* **2010**, *12*, 1724–1732.
[13] a) F. M. Liu, J. H. Jia, L. D. Zhang, *Appl. Phys. A* **2000**, *70*, 457–459; b) G. P. Schwartz, G. J. Gualtieri, W. A. Sunder, L. A. Farrow, *Phys. Rev. B* **1987**, *36*, 4868–4877.
[14] a) W. E. Morgan, W. J. Stec, J. R. Van Wazer, *Inorg. Chem.* **1973**, *12*, 953–955; b) R. J. Iwanowski, M. Heinonen, I. Pracka, J. Raczyńska, K. Fronc, J. W. Sobczak, *J. Alloys Compd.* **1999**, *286*, 162–166.
[15] a) F. M. Liu, L. D. Zhang, *Semicond. Sci. Technol.* **1999**, *14*, 710–714; b) Z. Y. Liu, B. Hawkins, T. F. Kuech, *J. Vac. Sci. Technol. B* **2003**, *21*, 71–77; c) Z. Y. Liu, T. F. Kuech, D. A. Saulys, *Appl. Phys. Lett.* **2003**, *83*, 2587–2589.
[16] J. H. Dias da Silva, S. W. da Silva, J. C. Galzerani, *J. Appl. Phys.* **1995**, *77*, 4044–4048.
[17] a) K. D. Childs, B. A. Carlson, L. A. LaVanier, J. F. Moulder, D. F. Paul, W. F. Stickle, D. G. Watson in *Handbook of Auger Electron Spectroscopy* (Ed.: C. L. Hedberg), Physical Electronics Inc., Minnesota, **1995**, pp. 178–181; b) C. Palacio, J. Olvera, J. L. Plaza, E. Diéguez, *Surf. Coat. Technol.* **2012**, *206*, 3146–3150; c) M. Pérotin, P. Coudray, L. Gouskov, H. Luquet, C. Llinarés, J. J. Bonnet, L. Soonckindt, B. Lambert, *J. Electron. Mater.* **1994**, *23*, 7–12.

Received: May 26, 2015
Published online: August 18, 2015

